Sensitivity of front-face weld geometry in representing the full penetration

Y M Zhang,* PhD
National Laboratory for Welding, Harbin Institute of Technology, Harbin, People's Republic of China

R Kovacevic, PhD, SME
Center for Robotics and Manufacturing Systems and Department of Mechanical Engineering, University of Kentucky, USA

L Wu, PhD
National Laboratory for Welding, Harbin Institute of Technology, Harbin, People's Republic of China

The measurement of weld penetration using a front-face sensor has been an important issue in welding automation. The fundamental problem is to find a measurable front-face parameter that can adequately represent the weld penetration. In this paper, both the front-face average weld depression depth (a novel weld geometrical parameter) and the weld width are selected as possible representations of full penetration in GTA welding. Two types of sensitivities of front-face weld geometry, with respect to variations in welding conditions and with respect to control variables, are proposed as criteria for determination of promising parameters. Sensitivity calculation of experimental data shows that the front-face weld width is not promising while the average front-face weld depression depth is. This conclusion is also confirmed by a specific experiment and statistic models.

1 INTRODUCTION

The measurement of weld penetration is a fundamental technique in closed-loop control of weld quality. A number of concepts have been presented to construct measurement mechanisms. These concepts include weld pool oscillation (**1–4**), ultrasonic sensing (**5–7**), infra-red sensing (**8–9**), bead width sensing (**10, 11**), radiographic sensing (**12, 13**), back-face bead sensing (**14, 15**) and back-face infra-red sensing (**16**), etc. The first four concepts are based upon front-face sensing, which is of interest here.

For pool oscillation, it has been shown by Hardt and others that it is impractical to measure the shape of a partial penetration pool (**2, 3**) and that it is unreliable to measure the shape of a full penetration pool if no other additional information is provided (**4**). In the case of ultrasonic sensing, contact transducers have been used (**6, 7**) which are inconvenient in practical welding. Of the existing front-face sensing techniques, the infra-red approach is probably the most promising. However, the empirical relationship, which can be used to calculate the weld penetration state from the infra-red images, was obtained without consideration of variations in welding conditions (**9**). In fact, the closed-loop control of weld penetration is primarily motivated by the influence of variations in welding conditions upon the weld penetration states. (If no variation in welding conditions existed, open-loop control would be adequate.). Therefore, such relationships must be acquired with consideration of variations in welding conditions.

In the present study the full penetration is concerned, the state of which is described by the back-face weld width b_b (see Fig. 1). A front-face three-dimensional vision-based full penetration sensing technique is proposed to monitor the full penetration from the front-face. In order to determine the front-face presentation of b_b, the possible representations are first proposed, which are the average front-face weld depression depth h and the front-face weld width b (see Fig. 1). Since the final representations must be sensitive to the control variables (the welding current and the arc length) and variations in welding conditions, the sensitivity analysis has been conducted to select the promising candidates based on the experimental data generated from various welding conditions.

The MS was received on 5 May 1992 and was accepted for publication on 17 June 1992.

* *Present address: Center for Robotics and Manufacturing Systems, University of Kentucky, USA.*

2 SENSITIVITIES

Two types of sensitivities, with respect to the variations in welding conditions and to control variables, are defined in this section.

2.1 Disturbance sensitivity S_D

This is a measure of sensitivity with respect to possible disturbances in weld conditions. Suppose that experiments are conducted under M types of possible welding conditions. The outputs in experiment k ($k = 1, \ldots, M$) are denoted by $b_k(i)$ and $h_k(i)$ where ($i = 1, \ldots, N$) is the

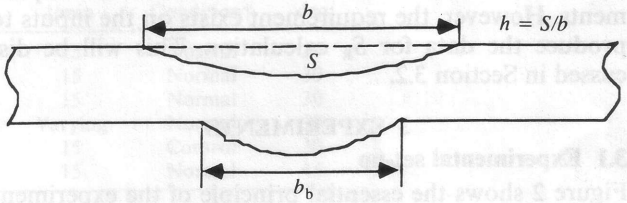

Fig. 1 Cross-section of a full penetration weld

0954-4054/92 $3.00 + .05

sampling instant. We define:

$$S_D^{(h)} = \frac{\sum_{i=1}^{N}\sum_{k=1}^{M}\{h_k(i) - \bar{h}(i)\}^2/MN}{\bar{h}^2} \quad (1)$$

where

$$\bar{h}(i) = \frac{\sum_{k=1}^{M} h_k(i)}{M} \quad (2)$$

$$\bar{h} = \frac{\sum_{i=1}^{N}\bar{h}(i)}{N} = \frac{\sum_{i=1}^{N}\sum_{k=1}^{M} h_k(i)}{MN} \quad (3)$$

as the disturbance sensitivity of the depression depth h. For the disturbance sensitivity of the weld width, $S_D^{(b)}$, a similar definition may be made.

In the computational procedure for $S_D^{(h)}$, the means of the depression depth h at each single sampling instant i ($i = 1, \ldots, N$), $\bar{h}(i)$, are first calculated. Therefore, $(1/M)\sum_{k=1}^{M}\{h_k(i) - \bar{h}(i)\}^2$ can simply be regarded as a measure of deviation of the depression depth caused by the variations in welding conditions at instant i. $S_D^{(h)}$ is a standardized mean of such deviations with respect to possible sampling instants. Thus, $S_D^{(h)}$ is virtually an average degree of h distribution.

2.2 Response sensitivity S_R

Response sensitivity is a measure on the control capability of the selected control variables to h or b. The motivation to present S_R is to compare possible candidates from the point of view of regulation ability. If the selected representation can not be sufficiently regulated by control variables, either the representation or the control variables should be selected again.

Suppose that the inputs have been designed to excite the system dynamics. The response sensitivity of h can be defined as

$$S_R^{(h)} = \frac{\sum_{k=1}^{M}\left(\frac{1}{N}\left[\sum_{i=1}^{N}\{h_k(i) - \bar{h}_k\}^2/\bar{h}_k^2\right]\right)}{M} = \frac{\sum_{k=1}^{M} S_R^{(h)}(\text{experiment } k)}{M} \quad (4)$$

where

$$\bar{h}_k = \frac{\sum_{i=1}^{N} h_k(i)}{N} \quad (5)$$

For the response sensitivity of b, the definition will be similar.

Note that there are virtually no requirements on experimental conditions to produce S_R. Therefore, a response sensitivity may be calculated for each single experiment. The final value calculated through equation (4) is the mean of the values from individual experiments. However, the requirement exists on the inputs to produce the data for S_R calculation. This will be discussed in Section 3.2.

3 EXPERIMENTS

3.1 Experimental set-up

Figure 2 shows the essential principle of the experimental set-up. An Nd: YAG laser of 1.06 μm and an optical

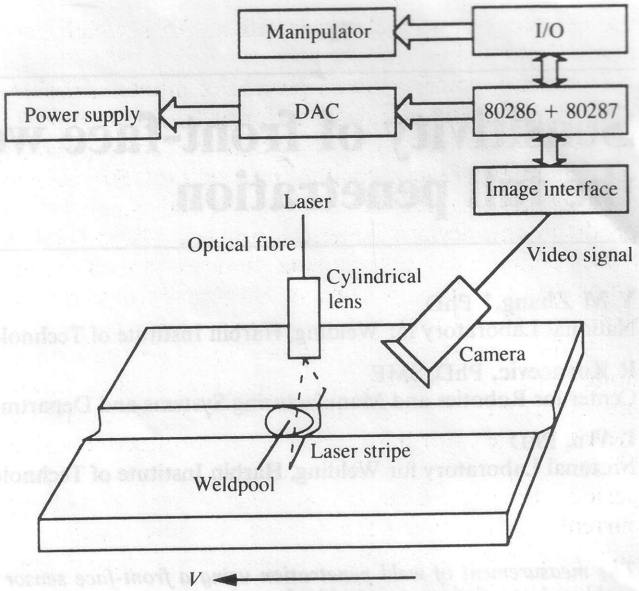

Fig. 2 Experimental set-up principle

lens produce the structured-light plane. A narrow-band optical filter with 123 Å half-width together with a camera (National V-260) is used to obtain the structured-light three-dimensional image of weld with a laser stripe. The image is sampled and transformed into 512 × 512 × 8 bits digital greyscale matrix by a real-time image interface of unique design. The sampling and transforming are performed in real time. The image processing algorithm (**17**) runs at 5 Hz. The computer is an IBM PC/AT with an 80287 math co-processor. The welding equipment consists of a constant-current rectified a.c. power supply, with a range of 60–350 A, and an air-cooled GTAW torch operating in a d.c. electrode negative mode. The welding current instruction is set by the computer through a 12 bit digital-to-analogue converter (DAC). For our experiments, the instructions for both the welding current and the arc length are pre-programmed (the torch travel velocity is constant). All of the computations of the dynamic experiment [including giving input instructions, sampling and transforming the image, processing the digital greyness matrix and storing the computed results, that is $h(k)$ and $b(k)$] are performed in real time.

3.2 Experimental design

It is likely that constant welding parameters (welding current i and arc length l) will be adequate to produce the experimental data to calculate S_D. However, for S_R calculation, variations in welding parameters are required to excite the system dynamics. This requirement is similar to that for the input design in dynamic system identification. In the following discussion, the sampling period and the input spectrum (**18**) will be addressed, while the time period is chosen to be 100 seconds, based upon the length of the experimental test-pieces and the torch velocity.

Consider the sampling period T. A proper choice of sampling period in most cases is not critical due to the relatively wide possible range between the values, which is too small or too large. Good results have been obtained using the rule $T_{95}/T = 5 \sim 15$ where T_{95} is the 95 per cent settling time of a transient process. In our case, T_{95} of the response of h to step i is 4 ~ 6 s. Thus,

the sampling period T is selected as 0.5 s which produces $T_{95}/T = 8 \sim 12$.

In order to specify the amplitude of inputs, a preliminary experiment should be performed to determine an operating point that can maintain the corresponding outputs (h and b) at a roughly proper level. Subsequent experiments can determine the permitted range, which produces the desired penetration state. The results of these preliminary experiments indicate an operating point $i_0 = 120$ A, $l_0 = 3$ mm and a permitted range 105 A $\leqslant i \leqslant$ 135 A, 1 mm $\leqslant l \leqslant$ 5 mm.

As the first step, two independent Gaussian white noise sequences with the operating point as their means are considered as the inputs. However, because the inertia of the system is too large to produce a visible effect of inputs upon outputs during a single sampling period, the minimum maintained time of welding current, during which the current remains constant, is increased from 1 sampling period to 5. Figure 3 contains the final input design.

3.3 Experimental conditions

All the weldments were produced in type 321 austenitic stainless steel (18Cr–9Ni–Ti) and have dimensions of 100 mm in width, 250 mm in length and 2 mm in thickness. The electrode is 2 per cent thoriated tungsten 3 mm in diameter. The torch velocity is 2 mm per second. High-purity argon gas is employed as the shielding gas.

In order to investigate the disturbance sensitivity, experiments must be conducted under different welding conditions. These experiments should emulate the welding condition variations of interest. These interest variations are unknown with respect to the feedback control system. (Known variations in welding conditions can usually be overcome by experimentally selected parameters. The primary objective of the feedback control system is to depress the influence of the unknown variations.)

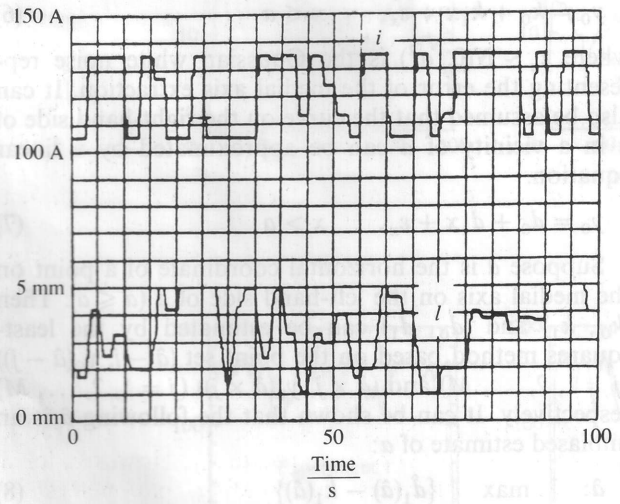

Fig. 3 Input signals for dynamic experiments

The unknown variations may be caused by electrode wear, environmental temperature or heat-transfer conditions, irregularity of the gap between the plates to be joined, variation in the rate of shielding gas flow, etc. The composition of the material, thickness of the workpiece, diameter of the electrode, etc., are regarded to be known and will not be considered in the experiments. In respect to the above, six typical welding conditions have been selected as shown in Table 1.

In Table 1, the description 'natural gap' for the gap between two plates to be joined is used. This description simply means that these two plates are cut in an ordinary fashion and then directly placed together. With consideration of variation in gap, three types of gap have been considered: no gap (bead-on-plate in experiment 1), butt welding with a natural gap (experiment 2) and a gradually varying gap from 0 to 0.5 mm (experiment 3). For the sake of gap control, spot welding has been performed to pre-join the two plates to be joined in advance. In order to emulate the variation in the rate of shielding gas flow, a varying rate is used in experiment 4, as shown in Fig. 4. In experiment 5, the heat-transfer condition is made different from the others by drilling ten holes (15 mm in diameter) in the workpiece. The centres of these holes are 20 mm from the joint path. These holes cause the heat-transfer condition to become poorer than the others where no holes exist. Also, the heat-transfer condition becomes even poorer by inserting asbestos cloth between the weldment and the fixture. Finally in experiment 6, the angle of the electrode tip is selected to be 45°. In other experiments, 30° has been used.

3.4 Image processing

Figure 5 shows a typical weld-stripe image from the vision sensor during welding. Processing of such an image will produce the weld geometrical parameters. Details of the image processing technique is discussed in reference (**17**). In this section, a short description of the technique is given.

The procedure of real-time image processing is: (a) adaptive extraction of the medial axis $y = y_0(x)$ (see Fig. 6); (b) unbiased recognition of the feature points

Table 1 Typical welding conditions

Experiment number	Position	Gap	Flow* l/min	Condition†	θ‡ deg
1	Bead-on-plate	No	15	Normal	30
2	Butt	Natural	15	Normal	30
3	Butt	0.5 mm	15	Normal	30
4	Butt	Natural	Varying	Normal	30
5	Butt	Natural	15	Control	30
6	Butt	Natural	15	Normal	45

* Rate of argon flow.
† Heat-transfer condition.
‡ Electrode tip angle.

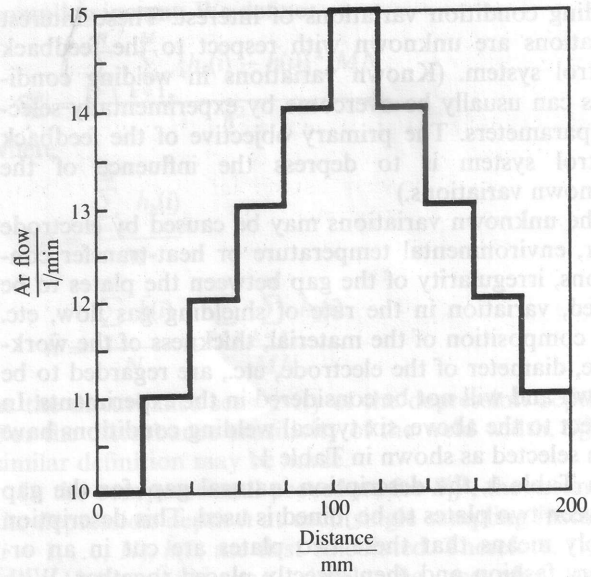

Fig. 4 Rate of argon flow in experiment 4

$(a, y_0(a))$ and $(b, y_0(b))$ (see Fig. 6); (c) computation of the weld geometric parameters.

In order to promote the computational speed, a dynamic thinning procedure (DTP) is proposed based upon the assumption that the laser stripe is continuous. The essence of this procedure is to begin the search for the maximum greyscale point (the set of which along the x axis is selected to be the medial axis of the laser stripe) from an initial point that is close to the maximum greyscale point. According to the assumption on the continuity, the vertical coordinate of this initial point can be selected to be the vertical coordinate of the neighbouring maximum greyscale point, which is readily available. Thus, if the assumption on the continuity of the laser stripe is true, no more maximum greyscale points are located over a large range except the first one found in each frame image. The computational time will be significantly reduced. A revised algorithm has been proposed to overcome the influence of the discontinuity of the laser stripe (**17**). The resulting medial axes for the typical image can be found in Fig. 7.

Experiments reveal the revised algorithm to be robust to the various disturbances encountered during actual welding. Also, this algorithm can be implemented sufficiently fast to be regarded as real time for measurement.

Fig. 5 Typical laser stripe

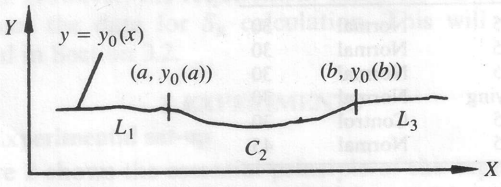

Fig. 6 Medial axis and its feature points

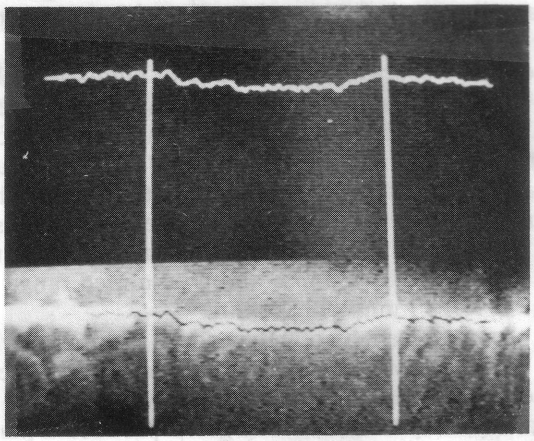

Fig. 7 Processing of image

The medial axis curve consists of three parts: two straight lines and a curve. The curve corresponds to the weld depression and the two straight lines correspond to the unmolten part of the weld. These three parts are divided by two points, called the feature points of the medial axis. In order to compute the weld geometric parameters accurately, the feature points must be recognized unbiasedly.

Assume a medial axis as shown in Fig. 6. The intention here is to determine the horizontal coordinates of the feature points $(a, y_0(a))$ and $(b, y_0(b))$, that is a and b. In the following discussion, only a is considered since b can be recognized in the same manner.

Suppose the equation of the straight line on the left-hand side of a is

$$y_0 = k_0 + k_1 x + \varepsilon_x, \qquad x \leqslant a \tag{6}$$

where $\varepsilon_x \sim N(0, \sigma^2)$ is the Gaussian white noise representing the error of the medial axis extraction. It can also be assumed that the curve on the right-hand side of a in a vicinity of a can be approximated by a linear equation.

$$y_0 = d_0 + d_1 x + \varepsilon_x, \qquad x > a \tag{7}$$

Suppose $\hat{a}$ is the horizontal coordinate of a point on the medial axis on the left-hand side of a ($\hat{a} \leqslant a$). Then (k_0, k_1) and (d_0, d_1) can be estimated by the least-squares method based on the point set $(\hat{a} - j, y_0(\hat{a} - j))$ $(j = 1, 2, \ldots, M)$ and $(\hat{a} \times j, y_0(\hat{a} \times j))$ $(j = 1, 2, \ldots, M)$ respectively. It can be shown that the following $\hat{a}$ is an unbiased estimate of a:

$$\hat{a}: \max_{\hat{a} \in (a-M,\, a+M)} \{\hat{d}_1(\hat{a}) - \hat{k}_1(\hat{a})\} \tag{8}$$

Thus, an unbiased recognition algorithm for feature points can be obtained. The resulting algorithm costs about 12 ms. Therefore, the recognition algorithm for the feature points is of real time as well for the present problem.

The three parts of the medial axis are then fitted to a linear, a quadratic and a linear model utilizing the least-squares method respectively, progressing from left to right on the image. Suppose the resulting models are $l_1(x)(x \leqslant a)$, $c_2(x, x^2)(a < x < b)$ and $l_3(x)(x \geqslant b)$ respectively (see Fig. 6). The point of intersection of l_1 and c_2 is (a^*, y_1^*); the point of intersection of c_2 and l_3 is (b^*, y_2^*). Denote the straight line connecting (a^*, y_1^*) and

(b^*, y_2^*) as l_2. Then the following equations to compute the weld geometric parameters of interest can be employed:

Weld width:

$$b^* - a^* \tag{9}$$

Average depression depth:

$$\frac{\int_{a^*}^{b^*} (l_2 - c_2)\, dx}{b^* - a^*} \tag{10}$$

Experiments have shown that the present real-time processing algorithm functions well during actual welding where various noises are sometimes present. Figure 7 illustrates the results of the extracted medial axis and the feature points for the typical image. The total time for the image sampling, the image processing and the weld geometric computation is less than 200 ms on this experimental set-up. The on-line measurement results of the dynamic experiments are depicted in Fig. 8. The sampling interval is 1 mm (corresponding to 0.5 s). The units for h and b are $\text{pixel}_y = 0.0436$ mm and $\text{pixel}_x = 0.05$ mm respectively. These units are the resolutions of the image system along the weld depression depth and the weld width directions respectively. From Fig. 8 it can be seen that similar curves have been acquired in different experiments. This is due to the fact that the same input signals have been employed. However, because of the variations in welding conditions in different experiments, discrimination exists as well. The data in Fig. 8 will be utilized to calculate the sensitivities in the next section.

4 RESULTS AND DISCUSSION

In order to remove the influence of the beginning and rear portions, take the data in the interval (11 mm, 190

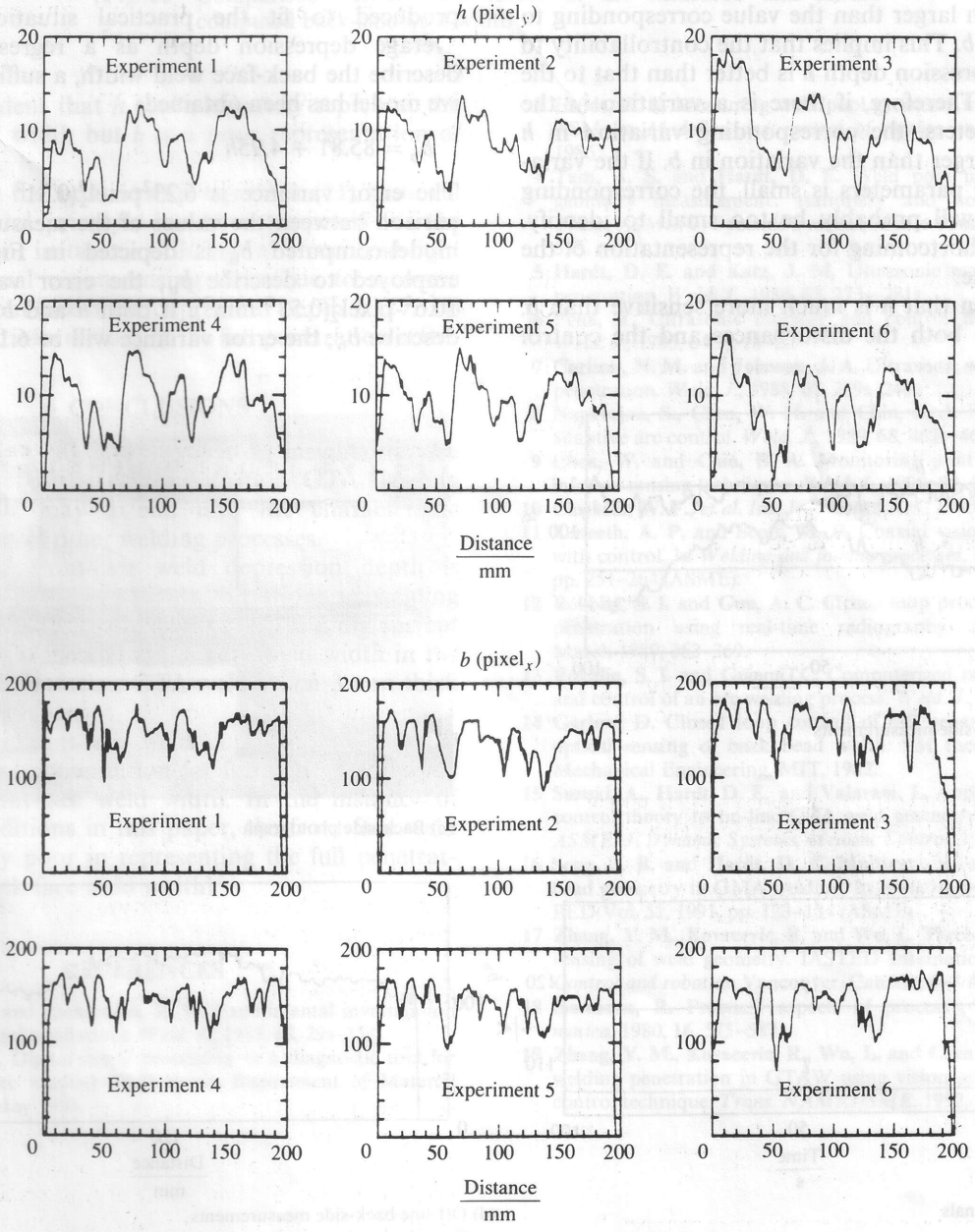

Fig. 8 Outputs of dynamic experiments

mm). The following can be yielded:

$$S_D^{(h)} = 0.1596^2$$

$$S_D^{(b)} = 0.0806^2$$

$$\frac{S_D^{(h)}}{S_D^{(b)}} = 3.88$$

It is evident that under the same welding condition disturbances the disturbance sensitivity of the average depression depth h is much larger than the value corresponding to weld width. Hence, the average depression depth is more sensitive to the welding condition variations or disturbances.

Similarly, the following can be obtained:

$$S_R^{(h)} = 0.1182$$

$$S_R^{(b)} = 0.0230$$

$$\frac{S_R^{(h)}}{S_R^{(b)}} = 5.14$$

Thus, the response sensitivity of the average depression depth h is much larger than the value corresponding to the weld width b. This implies that the controllability to the average depression depth h is better than that to the weld width b. Therefore, if there is a variation in the welding parameters, the corresponding variation in h will be much larger than the variation in b. If the variation in welding parameters is small, the corresponding variation in b will probably be too small to identify. This is also a shortcoming for the representation of the penetration state.

It can be seen that h is much more sensitive than b, with respect to both the disturbances and the control variables. This is a characteristic of the full penetration GTA welding process. Of course, this conclusion is based on the specific condition described in Section 2.

The experiment shown in Fig. 9 may be an example to illustrate the sensitivity characteristics in this instance. In this experiment, the workpiece is machined to emulate the variation in the heat-transfer condition. It can be seen that the variation in b caused by the heat-transfer condition is not apparent while the corresponding variation in h is significant.

5 APPLICATION

According to the aforementioned results, the average depression depth should be selected from the point of view of measurability of the variations in disturbance and control variables.

The measured b_b values are produced in five experiments which are designed to yield data to obtain the relationship between the front-face geometry and the back-face weld width. Here much smoother data are produced to fit the practical situation. Using the average depression depth as a regressive factor to describe the back-face weld width, a sufficiently regressive model has been obtained:

$$b_b = 85.81 + 4.95h \tag{11}$$

The error variance is $6.23^2\text{pixel}_x^2(0.31^2\ \text{mm}^2)$. A comparison between the values of the measured b_b and the model-computed b_b is depicted in Fig. 10. If b is employed to describe b_b, the error variance will be $10.6^2\text{-pixel}_2^2(0.53^2\ \text{mm}^2)$. If both h and b are utilized to describe b_b, the error variance will be $6.10^2\text{pixel}_x^2(0.305^2$

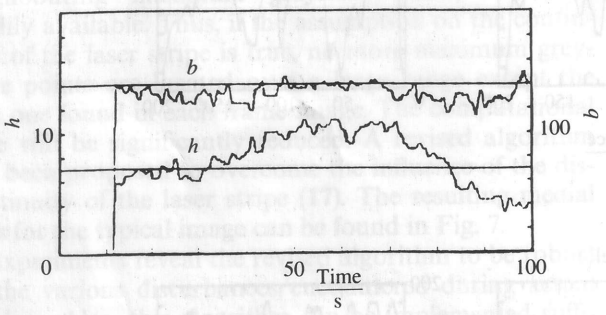

(a) On-line top-side measurements

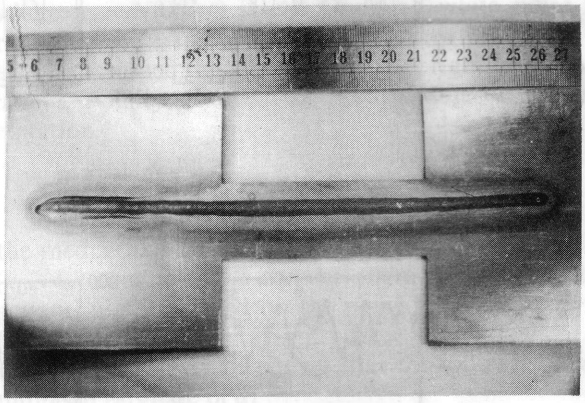

(c) Back-side photograph

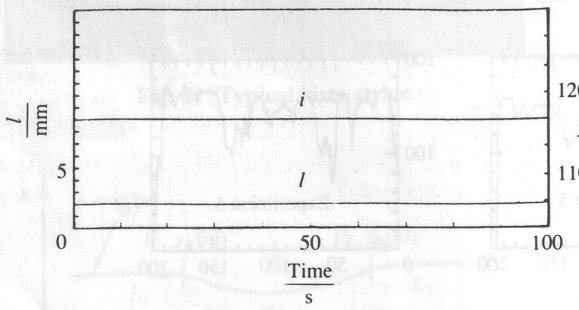

(b) Control signals

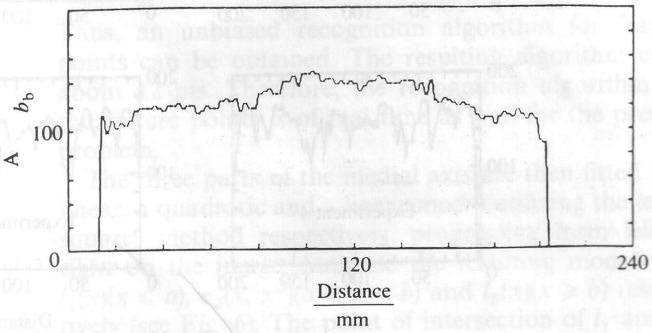

(d) Off-line back-side measurements

Fig. 9 Bead-on-plate experiment under varying heat-transfer conditions

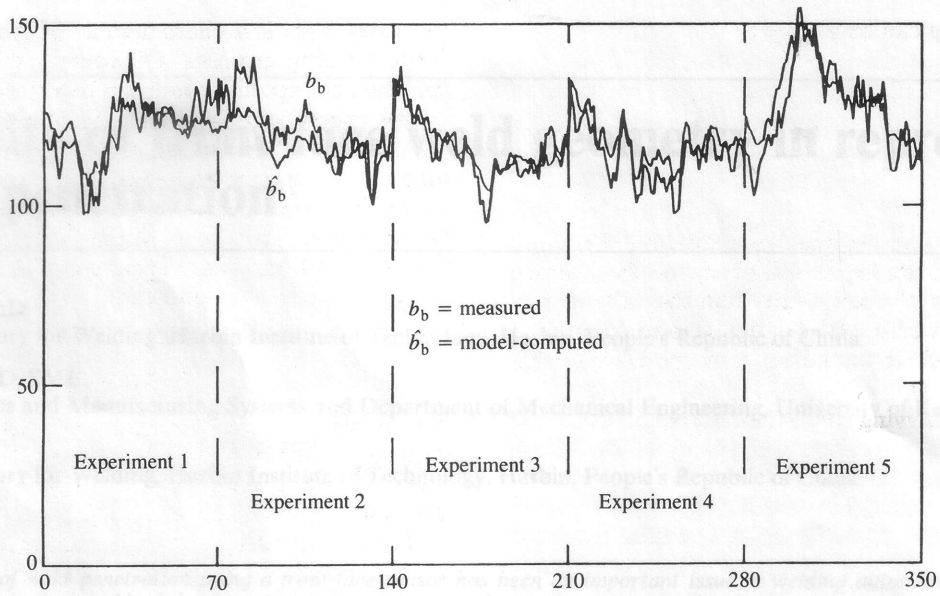

Fig. 10 Comparison between the values of the measured and model-computed back-side weld width

mm^2). It is evident that h can adequately represent the back-face weld width but b is a poor representation of the weld width.

Based upon the relationship equation (11), a novel front-face control principle has been proposed for the full penetration instance, utilizing a structured-light three-dimensional vision-sensing technique to measure the average front-face weld depression depth h (**17**, **19**) as the feedback information of the full penetration state.

6 CONCLUSIONS

1. Sensitivity analysis may provide an insight into the characteristic of the full penetration GTA welding process. This may extend into the characteristic investigations of other welding processes.
2. The average front-face weld depression depth is much more sensitive to both variations in welding conditions and the control variables (welding current and arc length) than the front-face weld width in the case of full penetration GTA welding on 3 mm thick stainless steel plates.
3. The average front-face weld depression depth is a much better representation for full penetration state than the front-face weld width. In the instance of welding conditions in this paper, the front-face weld width is very poor in representing the full penetration state (back-face weld width).

REFERENCES

1 **Renwick, R. J.** and **Richardson, R. W.** Experimental investigation of GTA weld pool oscillations. *Weld. J.*, 1983, **62**, 29s–35s.
2 **Sorensen, C. D.** Digital signal processing as a diagnostic tool for gas tungsten arc welding. PhD thesis, Department of Material Science, MIT, May 1985.
3 **Hardt, D. E.** Measuring weld pool geometry from pool dynamics. ASM on *Modeling and control of casting and welding*, January 1986.
4 **Tam, A. S.** and **Hardt, D. E.** Weld pool impedance for pool geometry measurement: stationary and nonstationary pools. *Trans. ASME, J. Dynamic Systems, Meast Control*, 1989, **111**, 545–553.
5 **Hardt, D. E.** and **Katz, J. M.** Ultrasonic measurement of weld penetration. *Weld. J.*, 1984, **63**, 273s–281s.
6 **Fenn, R.** Ultrasonic monitor and control during arc welding. *Weld. J.*, 1985, **64**(9), 18–22.
7 **Carlson, N. M.** and **Johnson, J. A.** Ultrasonic sensing of weld pool penetration. *Weld. J.*, 1988, **67**, 239s–246s.
8 **Nagarajan, S., Chen, W. H.** and **Chin, B. A.** Infrared sensing for adaptive arc control. *Weld. J.*, 1989, **68**, 462s–466s.
9 **Chen, W.** and **Chin, B. A.** Monitoring joint penetration using infrared sensing techniques. *Weld. J.*, 1990, **69**, 181s–185s.
10 **Clocksin, W. F.,** *et al. Int. J. Robotics Res.*, 1985, **4**(1), 13–26.
11 **Kenneth, A. P.** and **Scott, M. P.** Coaxial vision-based weld pool with control. In *Welding and joining processes*, PED Vol. 51, 1991, pp. 251–264 (ASME).
12 **Rokhlin, S. I.** and **Guu, A. C.** Closed-loop process control of weld penetration using real-time radiography. *Mater. Evaluation*, March 1989, 363–369.
13 **Rokhlin, S. I.** and **Guu, A. C.** Computerized radiographic sensing and control of an arc welding process. *Weld. J.*, 1990, **69**, 83s–97s.
14 **Garlow, D.** Closed loop control of full penetration welds using optical sensing of back bead width. SM thesis, Department of Mechanical Engineering, MIT, 1982.
15 **Suzuki, A., Hardt, D. E.** and **Valavani, L.** Application of adaptive control theory to on-line GTA weld geometry regulation. *Trans. ASME, J. Dynamic Systems, Measmt Control*, 1991, **113**, 93–103.
16 **Song, J. B.** and **Hardt, D. E.** Multivariable adaptive control of bead geometry in GMA welding. In *Welding and joining processes*, PED Vol. 51, 1991, pp. 123–134 (ASME).
17 **Zhang, Y. M., Kovacevic, R.** and **Wu, L.** Three-dimensional vision sensing of weld geometry. IASTED International Conference on *Control and robotics*, Vancouver, Canada, 4–7 August 1992.
18 **Isermann, R.** Practical aspects of process identification. *Automatica*, 1980, **16**, 575–587.
19 **Zhang, Y. M., Kovacevic, R., Wu, L.** and **Chen, D. H.** Controlling welding penetration in GTAW using vision sensing and adaptive control technique. *Trans. NAMRI/SME*, 1992, **20**, 317–323.